The Eurasia Proceedings of Science, Technology, Engineering & Mathematics (EPSTEM)
ISSN: 2602-3199

The Eurasia Proceedings of Science, Technology, Engineering and Mathematics (EPSTEM), 2025

Volume 37, Pages 150-162

ICEAT 2025: International Conference on Engineering and Advanced Technology

Investigation of the Efficacy of Steel Section Reinforcement in Hybrid Deep Beam Applications

Hussain K. Hashim
University of Misan

Abdulkhaliq A. Jaafer
University of Misan

Hayder AL-Khazraji
University of Misan

Abstract: This research provides an experimental evaluation of the shear behavior of deep beams reinforced with alternative shear reinforcement systems. It also explores the optimal arrangement of concrete types within hybrid deep beams to reduce both material costs and structural weight while maintaining load-bearing capacity. A total of six specimens were prepared and categorized into two main groups. Group 1 (G1) included two control beams one fully cast with normal-strength concrete and the other with high-strength concrete both featuring identical reinforcement layouts. Group 2 (G2) comprised four hybrid beams that incorporated both normal- and high-strength concrete arranged in a triangular configuration guided by the Strut-and-Tie Model (STM). In all specimens, traditional strut reinforcement was replaced with 40×40×4 mm angle steel sections. Each beam measured 1200 mm in length, 500 mm in depth, and 150 mm in width. Under single-point loading with a consistent shear span-to-depth ratio (a/d = 1), the hybrid beams achieved a 75% increase in shear strength and a 235.6% enhancement in stiffness compared to the normal-strength control beam. Additionally, toughness and ductility improved by 77.5% and up to 116.4%, respectively. When compared with the high-strength control beam, the hybrid specimens still demonstrated capacity gains of up to 25.6%, along with notable improvements in stiffness, toughness, and ductility. These results underscore the advantages of hybrid concrete configurations and alternative reinforcement methods in enhancing deep beam performance.

Keywords: Deep beams, Hybrid deep beams, High strength concrete, Shear diagonal cracks, Steel section.

Introduction

Ensuring the structural integrity of concrete buildings is essential for the safety of their occupants. This can only be achieved through a thorough understanding of how concrete members resist external loads. Engineers can then design and reinforce these structures based on the specific function of each member. Research has shown that deep beams do not conform to Bernoulli's theory. Instead, different regions of deep beams experience varying stress distributions in some areas are subjected to simple stresses, while others endure concentrated tensile and compressive stresses (Fan et al., 2022; Silveira et al., 2022; Karimizadeh et al., 2021). To address these localized stress concentrations, reinforcement strategies have been developed to enhance their structural performance.

Several design theories have been proposed for deep beams. However, the (STM), as outlined in the ACI code (ACI, 318M-19), has proven to be the most accurate and safest, with the lowest deviation from experimental results. While conservative, STM has shown to be useful for examining deep beams made of reinforced concrete

- Selection and peer-review under responsibility of the Organizing Committee of the Conference

(Yang et al., 2011; Abdul-Razzaq et al., 2017; Abdul-Razzaq et al 2020). For example, (Mohammedali et al, 2019) tested two full-scale continuous deep beams, each measuring 1700 mm in length with a constant cross-section of 140 mm by 500 mm. The design of the beams followed the (STM) technique based on (ACI 318-08), and they were subjected to a uniformly distributed load. The researchers found that the STM-predicted load (PSTM) was about 21% lower than the experimental ultimate load (P) for a single central load and about 27% lower for a uniform load. This discrepancy arises because, from the STM perspective, a safe load is one that balances internal and external stresses while remaining within the yield point (Abdul-Razzaq et al., 2018).

Research has continued to explore new methods for enhancing shear resistance, including the hybridization of concrete to reduce costs and the use of high-strength concrete to improve load-bearing capacity particularly in deep beams. Ahmed et al. (2021) examined the behavior of simply supported deep beams with layered concrete of different strengths (25 MPa and 50 MPa). They found that the optimal flexural performance was achieved when the bottom layer consisted of high-strength concrete. The deflection and failure load results were comparable to those of deep beams made entirely of high-strength concrete.

Shakir et al. (2023) introduced a novel hybridization model, referred to as the "curved model," where lightweight concrete was utilized below the contact zone and steel fiber concrete above it. This approach improved the beams' capacities by 23 and 27% under single-point and two-point loading conditions, respectively. More recently, Shakir et al. (2024) explored the use of recycled building materials to create cost-effective and environmentally sustainable deep beams. In their proposed model, the arch region was reinforced with steel fiber concrete, while the remaining sections incorporated recycled coarse aggregate (RCA) concrete. Their hybrid models demonstrated potential for reducing construction costs and mitigating the environmental impact of material waste. While previous studies have explored various hybridization techniques and reinforcement methods, they have not specifically investigated strengthening struts using steel sections or the addition of supporting ribs to enhance compressive resistance in these regions. The purpose of this study is to fill in current research gaps by implementing the following strategies:

- **Targeted Hybridization**: High-strength concrete (80 MPa) was utilized exclusively in the strut zones, cast in a triangular configuration, while the remaining portions of the beam were constructed using normal-strength concrete (25 MPa).
- **Steel Section Reinforcement**: Steel angle sections were employed in place of conventional reinforcement within the struts, functioning as compressed structural elements to improve shear capacity.
- **Tie Area Modification**: Selected reinforcement in the tie region was substituted with steel sections to assess their impact on the overall behavior of the beam.
- **Strut Midspan Ties**: The strut regions were interconnected at midspan to act as internal support, and the influence of this arrangement on the beam's structural performance was investigated.
- **Research Contribution**: Through these approaches, the study aims to advance the understanding of hybrid reinforcement strategies in deep beams and promote more efficient and resilient structural design methodologies.

Experimental Work

Specimens Description

The experimental program in this study involved testing six deep beams, divided into two groups, all subjected to an identical loading configuration. Each beam was tested under a single-point load, with uniform dimensions of 1200 mm in length, 500 mm in depth, and 150 mm in thickness. The shear span-to-depth ratio (a/d) was consistently maintained at 1.0 for all specimens.

The first and second beams served as control specimens, providing a basis for comparison with the remaining beams, which differed in terms of reinforcement strategies and concrete composition, as illustrated in Figure 1. Group 1 consisted of two control beams: the first was cast using normal-strength concrete (NSC) with a compressive strength of 25 MPa, while the second was made with high-strength concrete (HSC) with a compressive strength of approximately 85 MPa. Both control beams were reinforced with four Ø8 mm longitudinal steel bars and Ø4 mm stirrups spaced at 110 mm. Additionally, the struts in both beams were reinforced with two Ø12 mm and two Ø16 mm steel bars.

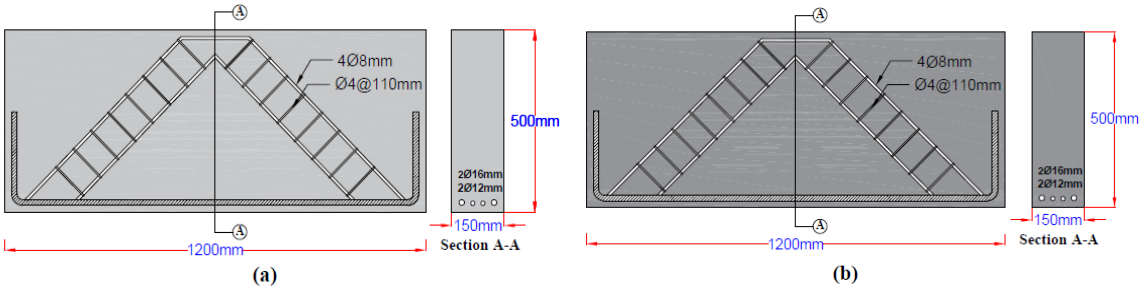

Figure 1. (a) G1-CO-1 (b) G1-CO-2.

For the second group specimens were hybrid deep beams with triangular-shaped concrete configurations, reinforced using L-shaped steel sections measuring 40×40×4 mm. In the first specimen, HSC was used in the strut zones only, while NSC was used in the remaining regions. The struts were reinforced with four L-steel sections, tied together with 30×4 mm steel plates via welding (see Figure 2(a)). The tie was reinforced with two Ø16 mm and two Ø12 mm steel bars. The second beam was designed similarly to the third but replaced the Ø16 mm bars in the tie zone with two L-steel sections to investigate their effect on the tensile strength of the deep beam (see Figure 2(b)). For the third and fourth beams, the same hybrid concrete layout was applied. However, only two L-steel sections tied together with steel plates were used in the struts. Additionally, a horizontal steel support was added between the two struts in the fifth beam (see Figure 2(c)). The sixth beam is shown in Figure 2(d). Both the fifth and sixth specimens used two Ø16 mm and two Ø12 mm steel bars in the tie region

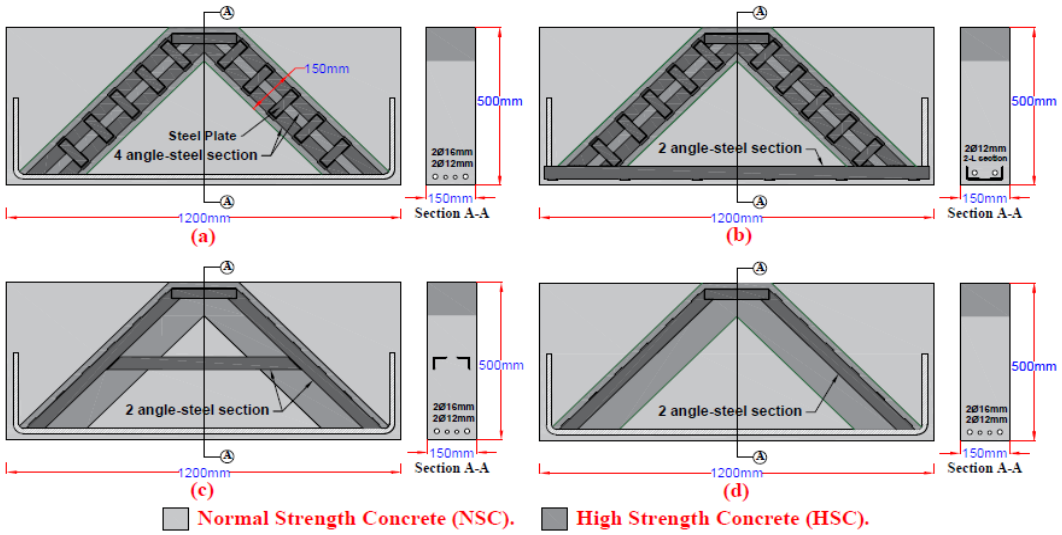

Figure 2. (a) G2-HT-S-1 (b) G2-HT-S-2 (c) G2-HT-S-3 (d) G2-HT-S-4

Materials Used in Experimental Work

Table 1. Grading of the used fine aggregates(sand).

Sieve Size(mm)	Percent of Passing%	Iraqi Specification IQ.S45/1984 for Zone (2)
10	100	100
4.75	97.8	90 - 100
2.36	88.8	75 - 100
1.18	75.4	55 - 90
0.6	57	35 - 59
0.3	26.6	8 - 30
0.15	3.4	0 - 10
Materials Passing through a sieve 75 micron %	4.2	≤ 5%

In this investigation, ordinary Portland cement (Crista) was used. The cement was tested physically, mechanically, and chemically in compliance with Iraqi Specification No. 5 (2019) to guarantee the accuracy and dependability of the experimental findings and to satisfy Iraqi standards. For normal-strength concrete (NSC),

full-grade sand with a maximum particle size of 4.75 mm was utilised, whereas for high-strength concrete (HSC), fine-grade sand with a maximum particle size of 1.18 mm was employed. Both sand kinds, as shown in Table 1, were confirmed to meet Iraqi Specification No. 45 (1984) and were sourced naturally inside the Basra Governorate.

Two grades of coarse aggregate were also employed. For (NSC), fully graded crushed gravel with a maximum size of 19 mm was used. For (HSC), natural crushed gravel with a maximum size of 12 mm was selected. All coarse aggregates were thoroughly washed and hand-sifted. According to Table 2, both types meet the requirements of (Iraqi Specification No.45, 1984). Both normal-strength and high-strength concrete mixes were prepared and cured using reverse osmosis (RO) water, which met the standards outlined in (Iraqi specifications 1703/2018). Mega Add MS(D), a high-performance pozzolanic mineral additive, was incorporated in the high-strength concrete mix. The silica fume characteristics provided by the manufacturer were in accordance with (ASTM C1240-03).

Sika ViscoCrete-180GS, a third-generation high-range water-reducing superplasticizer based on polycarboxylate polymer technology, was used to enhance concrete workability while maintaining high strength by lowering the water-to-cement ratio. Its properties conform to (ASTM C494/C494M-13). Four different diameters of reinforcing steel bars Ø16 mm, Ø12 mm, Ø8 mm, and Ø4 mm along with angle-shaped steel sections (40×40×4 mm), were used in this study. These materials complied with (ASTMA615/A615M-20 & ASTM/ E-28,2021), respectively. Table 3 provides the mechanical properties of the reinforcement bars and steel sections. Chinese welding wire, which is readily available in local markets and recognized as an acceptable welding material by the American Welding Society Standard (AWS, D.1978), was used to weld the steel sections.

Table 2. Grading of the used coarse aggregates.

Sieve Size (mm)	Percent of passing (%)	Iraqi Specification IQ.S45/1984 for Zone (2)
37.5	100	100
20	96.6	95 – 100
10	39.2	30 – 60
5	1.8	0 - 10
Materials Passing through a sieve 75 micron (%)	0.2	≤ 3%

Table 3. Properties of reinforcing bars and steel sections (average).

$D_{nominal}$ (mm)	Yield stress (N/mm^2)	Tensile stress (N/mm^2)
16	480	641
12	508	660
8	338	563
4	280	440
L-Section (40×40×4)	391	488
Steel plate (30×3)	432	524

Concrete Mix Design

Two mixers were used to prepare the two types of concrete separately, allowing them to be cast simultaneously to ensure proper bonding between them, in accordance with the mix proportions shown in Table 4 for each concrete type.

Table 4. Proportions concrete mixture.

No.	Materials	HSC (kg/m^3)	NSC (kg/m^3)
1	Cement	550	400
2	Water (%)	127 (20%)	212 (53%)
3	Gravel	1000	1064
4	Sand	800	656
5	Silica Fume	80	–
6	Superplasticizer, C+S (%)	12.6 (2%)	–

Tests of the Fresh Concrete

To guarantee the quality of the mixes during the casting of the main specimens, the workability of the concrete mixes used in this study was evaluated in accordance with (ASTMC143-17, 2017), as illustrated in Figure 3. The slump value for each mix is presented in Table 5.

Table 5. Slump test results of the tested concrete mixes.

No.	Type of concrete	Slump (mm)
1	HSC	135
2	NSC	205

Figure 3. Slump test for A) HSC and B) NSC.

Hardened Concrete's Mechanical Properties

Tests on hardened concrete were carried out in the University of Misan's College of Engineering research labs. Three 150×150×150 mm cubes were tested to determine the concrete's compressive strength in compliance with ASTM C31/C31M-21a (2021). Three 100×100×500 mm prisms were used to measure flexural strength in accordance with ASTM C78-09. According to ASTM C496/C496M-17 (2017), splitting tensile strength tests were performed on three cylindrical specimens: 150 x 300 mm for normal-strength concrete and 100 x 200 mm for high-strength concrete. Additionally, using 150×300 mm cylinders, the modulus of elasticity for both types of concrete was ascertained in accordance with ASTM C469-14. Table 6 provides a summary of these tests' outcomes.

Table 6. Test results hardened concrete.

Types of Concrete	Density (kg/m^3)	Compressive Strength, f_{cu}(MPa)	Flexural Strength (MPa)	Tensile strength, f_t (MPa)	Modulus of Elasticity, E_C(MPa)
HSC	2382.2	87.83	8.6	3.19	43076.21
NSC	2425.1	25.1	3.2	2.15	23025.2

Instrumentation for Testing and Testing Machine

Figure 4. Flexural test machine.

All specimens were tested using a flexural testing machine manufactured by ALFA Company, with a maximum load capacity of 600 kN, as illustrated in Figure 4. The machine was programmed to apply the load automatically at a constant, adjustable rate. To prevent localized failure and surface crushing of the concrete, a 1 cm-thick rubber pad was placed beneath the loading point and above the supports. The load was applied incrementally in 5 kN steps to facilitate controlled testing and allow for the observation of crack development. Crack propagation was monitored and marked using a whiteboard marker throughout the testing process.

To measure deflection, a Linear Variable Differential Transformer (LVDT) was placed at the mid-span of each specimen, enabling continuous monitoring of deflection throughout the loading process. Additionally, strain gauges were connected to a data acquisition system to capture internal concrete strains at various loading stages, facilitating a comprehensive evaluation of the structural behaviour up to failure. The test setup and the arrangement of the strain gauges are shown in Figures 5 and 6, respectively. All specimens were tested with a constant shear span-to-depth ratio (a/d = 1), and the clear span between the supports was 1000 mm.

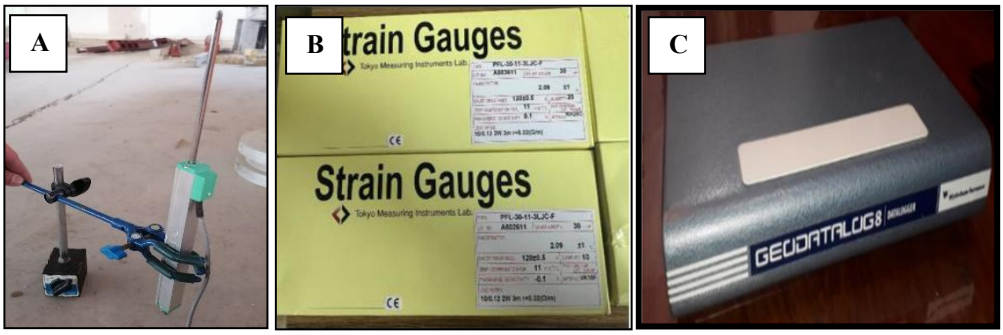

Figure 5. Devices of the test : A) LVDT, B) Strain gauges, and C) Data logger.

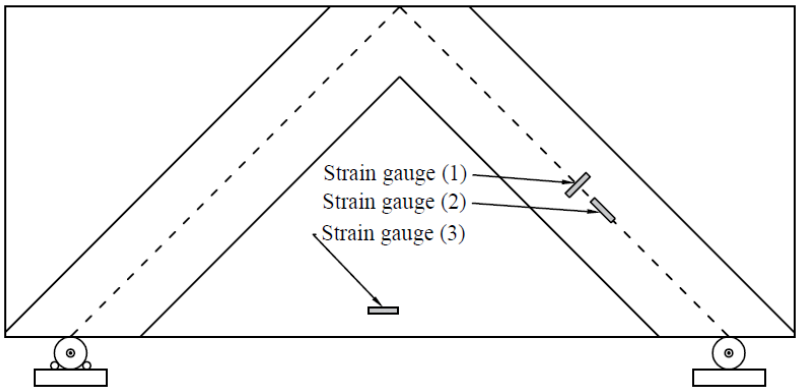

Figure 6. Strain gauges' location.

Results and Discussion

Table 7 shows the tested specimens, including the cracking load, ultimate load, maximum deflection, maximum strain, and mode of failure. Below is a detailed explanation of each specimen.

Table 7. Test results of the deep beam

Specimen	Load (kN) Cracking, P_{cr}	Ultimate, P_u	Max. deflection (mm)	Strain gauge (mm/mm) (1)	(2)	Mode of Failure
G1-CO-1	170	280	9.2	0.000871	0.00283	Nodal zone failure
G1-CO-2	180	390	7.445	0.000652	0.002025	Shear-semi flexural failure
G2-HT-S-1	150	490	6.612	0.00021	0.0031	Diagonal Shear failure
G2-HT-S-2	145	460	8.03	0.000232	0.002	Diagonal Shear failure
G2-HT-S-3	140	430	6.877	0.0004356	0.004048	Diagonal Shear failure
G2-HT-S-4	140	340	5.48	0.000155	0.004981	Diagonal Shear failure

Modes of Failure and Crack Propagation of the Specimens.

Figure 7 illustrates the failure modes of the control beams. The first crack appeared at 170 kN for the first control beam (G1-CO-1), and the beam reached a maximum load of 280 before failed by the nodal zone crushing, concrete strength (25.1 MPa). For the control beam (G1-CO-2), cast entirely with high-strength concrete (87.83 MPa), the first crack appeared at 180 kN. Cracks developed at the beam's mid-span bottom and the inner edge of the strut, leading to failure at 390 kN. The failure was a combination of shear and flexure, indicated by increased deflection under constant load suggesting yielding of the tie reinforcement and shear-induced cracking at the strut's inner edge. The behavior and capacity of the second group (G2) differed significantly from those of the first group (G1). In beam G2-HT-S-1, the first crack appeared at 150 kN earlier than in the control specimens. The beam continued to carry load until failure occurred at 490 kN due to diagonal shear failure in the strut region. Compared to the high-strength control beam (G1-CO-2), this reflects a 25.64% increase in the load bearing capacity, and a 75% increase compared to the normal-strength control (G1-CO-1).

Figure 7. Failure modes of the control beams (G1)

In beam G2-HT-S-2, the first crack appeared slightly earlier at 145 kN, with failure occurring at 460 kN due to diagonal shear, accompanied by crack development in the tie area. The reduced capacity may be attributed to the use of steel sections in the tie reinforcement. This beam showed capacity improvements of 64.28% and 18% compared to G1-CO-1 and G1-CO-2, respectively. For beam G2-HT-S-3, the first crack occurred at 140 kN. Steel sections were used on only one side, providing inadequate reinforcement to prevent strut crushing. This led to extensive cracking and shear failure at 430 kN, reflecting capacity increases of 53.57% and 10.25% relative to G1-CO-1 and G1-CO-2, respectively. Finally, beam G2-HT-S-4 showed no capacity improvement over G1-CO-2, with a 12.8% reduction. However, it still outperformed G1-CO-1 by 21.43%. The first crack appeared early at 140 kN, and the beam failed in shear at 340 kN following significant crack propagation and a major failure crack in the middle of the strut.

The early cracking in this group is attributed to the use of hybrid concrete. The use of hybrid concrete introduces internal stresses due to differences in shrinkage, elastic modulus, and thermal expansion, leading to early crack formation compared to uniform concrete, particularly at the interface between materials (Gao, Zhang, & Wang, 2014; Neville, 2011). However, the enhanced load-bearing capacity is due to the implementation of an effective (STM) and an innovative reinforcement approach using angle steel sections, which transform the strut into a compressive member capable of resisting high loads. Figure 8 show the crack propagation and the failure modes for the second group.

Figure 8. Modes of failure for the second group (G2)

Load-Midspan Deflection Curves

As for the first group (G1), the first beam (G1-CO-1) showed higher deflection than the second beam (G1-CO-2), as the value of deflection was 9.2mm and 7.445mm respectively, this due to use of normal strength concrete. In the second group, characterized by triangular hybrid reinforcement in the strut region, a significant improvement in both stiffness and load-bearing capacity was observed compared to the control specimens (G1-CO-1 and G1-CO-2). Figure 9 illustrates the load-midspan deflection curves, reflecting the structural response of each deep beam. The first beam (G4-HT-S-1) exhibited the most substantial increase in stiffness and load capacity, outperforming the control specimens throughout the entire loading process. It also recorded the lowest deflection at 6.612 mm. Although the second beam (G4-HT-S-2) showed lower performance than G4-HT-S-1, it still demonstrated notable improvements over the controls. It exhibited greater deflection (8.03 mm) and reduced stiffness and load capacity, likely due to partial replacement of tie reinforcement with angle steel sections, which may have affected confinement and load distribution. Beam G4-HT-S-3 displayed similar initial stiffness to G4-HT-S-2 but experienced a temporary increase in stiffness after initial cracking. However, beyond approximately 85% of the ultimate load, it suffered a loss in both stiffness and load-carrying capacity relative to G4-HT-S-2. Despite this, its deflection stayed less than the control specimens. The temporary improvement is likely due to stress redistribution facilitated by the midspan connection of struts using angle steel sections. The last beam (G4-HT-S-4) showed a slight early-stage stiffness improvement compared to the controls but suffered rapid stiffness degradation after secondary cracking. It ultimately failed due to abrupt diagonal shear at a lower load than (G1-CO-3). This premature failure is attributed to inadequate and asymmetrical reinforcement in the strut region, allowing the development of a weak path and rapid propagation of shear cracks. Overall, this group demonstrated that triangular hybrid reinforcement significantly enhances stiffness and load resistance when the strut region is adequately and symmetrically reinforced. The variations in performance among specimens emphasize how reinforcement is important, arrangement and confinement in influencing structural behavior under load. The experimental results suggest that the use of angle steel sections in the strut region can serve as an effective alternative to conventional reinforcement methods in deep beams. Beams in Group 4 (G4), which utilized triangular hybrid reinforcement incorporating angle steel within the strut zone, demonstrated significant enhancements in both stiffness and load-bearing capacity when compared to the control beams in Group 1 (G1).

This improvement is primarily attributed to the tight confinement and effective arrangement of the angle steel sections, which enhanced internal force transfer and delayed the onset of diagonal cracking. For instance, specimen G4-HT-S-1 achieved the lowest midspan deflection (6.612 mm) and the highest overall strength, indicating that properly integrated angle sections can create a robust internal strut mechanism that resists deformation efficiently. However, the reduced performance of specimens such as G4-HT-S-2 and G4-HT-S-4 underscores the importance of adequate and symmetrical reinforcement configuration. In G4-HT-S-4, the asymmetrical and insufficient reinforcement in the strut region led to premature diagonal shear failure, highlighting the critical role of reinforcement detailing.

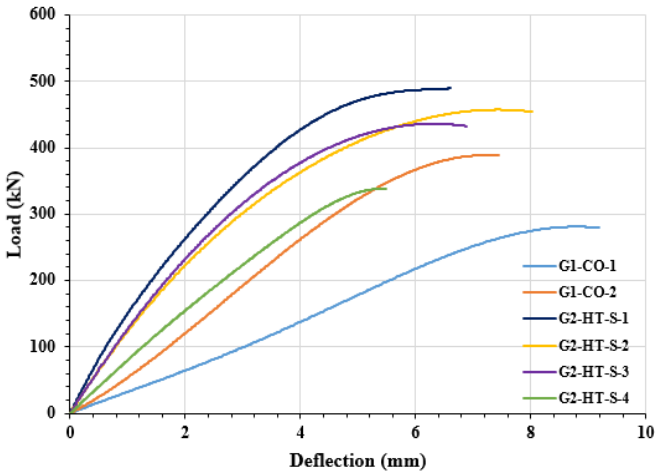

Figure 9. Load-Midspan deflection curves for the deep beams.

Overall, these findings indicate that angle steel sections can be a promising substitute for traditional reinforcement in the strut region, provided they are properly designed, symmetrically arranged, and well-confined. The performance variations observed among specimens further emphasize the influence of reinforcement detailing structural behavior under load.

Stiffness, Toughness and Ductility

Stiffness (K) refers to the resistance an elastic body offers to deformation. The "effective secant stiffness" at the load stage of 0.75 * Pu is used for evaluation (Park et al, 1988). The proposed specimens demonstrated significant improvements in stiffness relative to the control specimens (G1-CO-1 and G1-CO-2). Specifically, beam G2-HT-S-1 showed an increase of 235.6% and 77%, respectively; G2-HT-S-2 improved by 158.3% and 36.2%; G2-HT-S-3 increased by 201% and 58.8%; and G2-HT-S-4 improved by 100.6% and 5.76%. This enhancement in stiffness is attributed to the use of (HSC) and the inclusion of steel sections in the strut region, which together significantly improved the beams' resistance to deformation.

Toughness, symbolised by the region under the load-midspan Deflection curve, measures a member's resistance to deformation before failure (Shakir et al,2020). For the first group (G1), the toughness values were 21,579 kN·mm and 32,347 kN·mm for beams G1-CO-1 and G1-CO-2, respectively. In the second group (G2), beam G2-HT-S-1 exhibited toughness increases of 68% and 12% compared to G1-CO-1 and G1-CO-2, respectively. Similarly, beam G2-HT-S-2 showed improvements of 77.5% and 18.4% over the control specimens. For the third beam (G2-HT-S-3), the toughness value (29,776 kN·mm) was higher than that of G1-CO-1 but lower than that of G1-CO-2. Meanwhile, the final beam (G2-HT-S-4) demonstrated a lower toughness value (18,717 kN·mm) compared to both control specimens. Ductility (μ), which is represented by Eq. (1 (Naaman et al.,1995), is the ability to endure inelastic deformation till failure without lowering the ultimate load

$$\mu = 0.5 * (E_{tot}/E_{el} + 1) \quad (1)$$

The use of (HSC) combined with steel section reinforcement in the strut regions resulted in an enhancement of the ductility of the beams compared to the control specimens (G1). For the first beam (G2-HT-S-1), ductility increased by 89.65% and 71.86% relative to G1-CO-1 and G1-CO-2, respectively. The second beam (G2-HT-S-2) exhibited increases of 116.4% and 96%, while the third beam (G2-HT-S-3) showed improvements of 74.14% and 57.8%. The fourth beam (G2-HT-S-4) recorded increases of 20.7% and 9.38%, respectively. Table 8 and Figure 10 present the summarized results for stiffness, toughness, and ductility across all specimens.

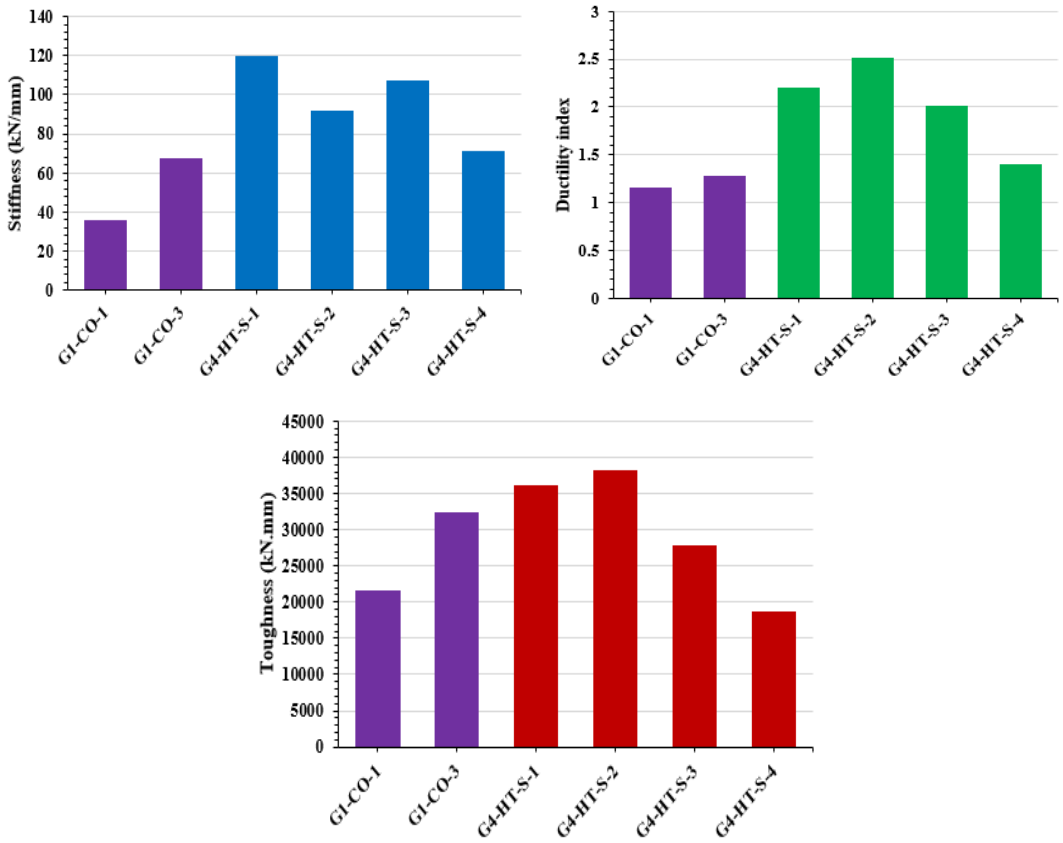

Figure 10. Results of stiffness, toughness and ductility for all tested specimens

Table 8. Results of stiffness, toughness and ductility for all specimens.

No.	Specimens	Stiffness (kN/mm)	Toughness (kN.mm)	Ductility
1	G1-CO-1	35.7	21,579	1.16
2	G1-CO-2	67.7	32,347	1.28
3	G2-HT-S-1	119.8	36,244	2.2
4	G2-HT-S-2	92.2	38,293	2.51
5	G2-HT-S-3	107.5	27,815	2.02
6	G2-HT-S-4	71.6	18,717	1.4

Concrete Surface Strain

To calculate the concrete surface strain, strain gauges were installed in two directions: one gauge (1) was positioned perpendicular to the longitudinal axis of the struts to measure tensile strain, and another gauge (2) was installed parallel to the axis to measure compressive strain (see Figure 6). The recorded readings are presented in Figure 11. The results from the tensile strain gauge indicate that all specimens in the second group (G2) exhibited lower strain values compared to the control specimens (G1), with tensile strain not exceeding 0.0004356 mm/mm. This reduction in strain is attributed to the use of steel sections that provided restraint to the struts, along with the application of high-strength concrete. The compressive strain results (measured by strain gauge 2) varied among the G2 specimens. For beam G2-HT-S-1, the strain was higher than the values recorded for the control specimens G1-CO-1 and G1-CO-2. Beam G2-HT-S-2 showed behavior and strain values closely matching those of G1-CO-2. Meanwhile, beams G2-HT-S-3 and G2-HT-S-4 exhibited higher compressive strain values compared to the control beams. To assess the effect of replacing part of the tie reinforcement with steel sections, a third strain gauge (3) was fixed at the midspan of the tie for beams G2-HT-S-1 and G2-HT-S-2. The findings proved that using steel sections in the tie region increased the concrete strain by approximately 25%. The use of steel sections in the reinforcement significantly reduced tensile strains due to improved confinement and restraint. Compressive strain behavior varied depending on reinforcement configuration.

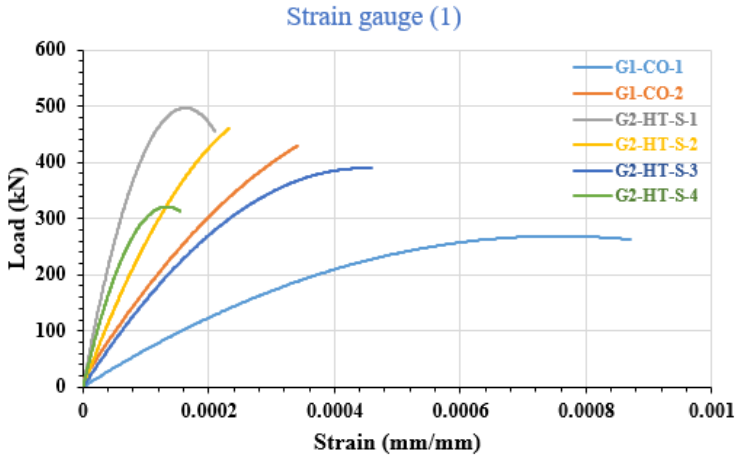

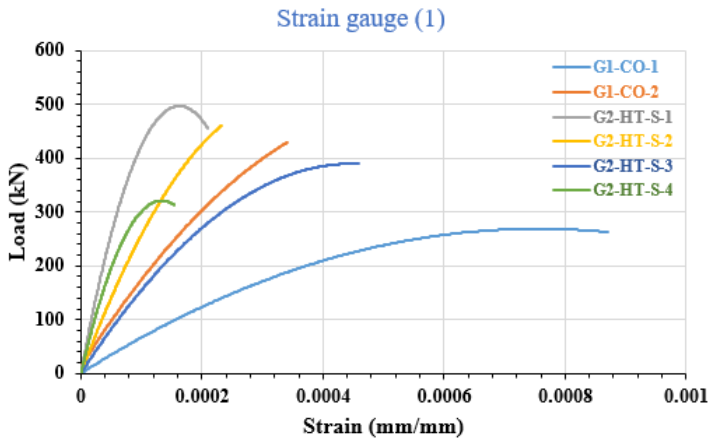

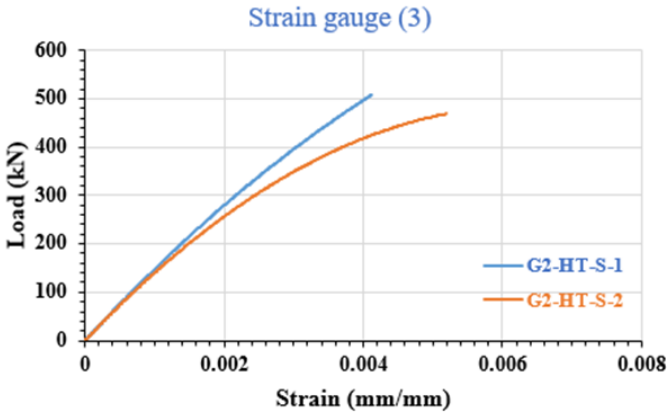

Figure 11. Results of strain value for strain gauge (1, 2 and 3).

Conclusion

The following points summarize the most important conclusions resulting from this research:

- In comparison to the first control beam, the suggested specimens' load-bearing capability increased by 75%, 64.28%, 53.57%, and 21.43% in the second group, respectively. Additionally, stiffness improved by 235.6%, 158.3%, 201%, and 100.6%, in that order. Toughness also increased by 28.9%, 77.5%, and 68%, respectively. Improvements in ductility were seen at 89.65%, 116.4%, 74.14%, and 20.7%, in that order.
- The suggested specimens' load-carrying capacities increased by 25.64%, 18%, 10.25%, and 12.8%, respectively, in comparison to the second control beam. The corresponding increases in stiffness were 77%, 36.2%, 58.8%, and 5.76%. Improvements in toughness were 12% and 18.25%, respectively. Ductility improvements were seen at 71.86%, 96%, 57.8%, and 9.38%, in that order.
- Without compromising the deep beams' shear performance, the use of HSC in the strut sections decreased material costs.
- There is a noticeable increase in ductility when angle steel sections are used as strut reinforcement components.
- The ultimate load capacity of the deep beams was increased by adding angle steel sections to the strut areas. It was discovered that angle steel sections were less successful when used in the tie zones.
- The overall capacity and structural behavior of the deep beams were unaffected by the use of (NSC) in the tie zones.

Recommendations

- The behavior of deep beams with openings should be investigated further in order to evaluate the reasons for failure and the performance of angle steel sections used to reinforce deep beams with openings.
- Effect of Arc-Shaped Strut Ridges: Studies should investigate the behavior of deep beams with arc-shaped strut regions.
- Effect of Different Ratios of (a/d): Researchers are encouraged to examine the impact of varying shear span-to-depth (a/d) ratios on the structural behavior of deep beams reinforced with angle steel sections.

Scientific Ethics Declaration

* The authors agree that they are responsible for the article's scientific, ethical, and legal responsibilities as published in the EPSTEM Journal.

Conflict of Interest

* No conflicts of interest are disclosed by the authors.

Funding

* Regarding the publishing of this work, the authors confirm that they have no conflicts of interest.

Acknowledgements or Notes

* This article was presented as an oral presentation at the International Conference on Engineering and Advanced Technology (ICEAT) held in Selangor, Malaysia on July 23-24, 2025.

References

Abdul-Razzaq, K. S., & Dawood, A. A. (2020). Corbel strut and tie modeling – Experimental verification. *Structures, 26*, 327–339.

Abdul-Razzaq, K. S., & Jebur, S. F. (2017). Experimental verification of strut and tie method for reinforced concrete deep beams under various types of loadings. *Journal of Engineering and Sustainable Development, 21*(6), 39–55.

Abdul-Razzaq, K. S., Jalil, A. M., & Mohammed, A. H. (2018). Applying various types of loading on continuous deep beams using strut and tie modelling. *International Journal of Engineering and Technology, 7*(4.2), 251–258.

Ahmed, N. A. M., Khalil, A. H. H., & Mostafa, E. E. D. (2021). Behavior of deep beams using different concrete grades. *International Research Journal of Innovations in Engineering and Technology, 5*(8), 75.

American Concrete Institute (ACI). (2019). *ACI 318M-19: Building code requirements for structural concrete and commentary*. American Concrete Institute.

American Welding Society (AWS). (1978). *Structural welding code – Steel (AWS D1.1)*. American Welding Society

ASTM A615/A615M-20. (2020). *Standard specification for deformed and plain carbon-steel bars for concrete reinforcement*. ASTM International.

ASTM C1240-03. (2003). *Standard specification for silica fume used in cementitious mixtures*. ASTM International.

ASTM C143-17. (2017). *Standard test method for slump of hydraulic-cement concrete*. ASTM International.

ASTM C31/C31M-21a. (2021). *Standard practice for making and curing concrete test specimens in the field*. ASTM International.

ASTM C494/C494M-13. (2013). *Standard specification for chemical admixtures for concrete*. ASTM International.

ASTM C496/C496M-17. (2017). *Standard test method for splitting tensile strength of cylindrical concrete specimens*. ASTM International.

ASTM C78-09. (2009). *Standard test method for flexural strength of concrete (using simple beam with third-point loading)*. ASTM International.

ASTM International Committee E28. (2021). *Standard test methods for tension testing of metallic materials*. ASTM International.

Central Organization for Standardization and Quality Control (COSQC). (2019). *Iraqi Specification No. 5: Portland cement*. COSQC.

Central Organization for Standardization and Quality Control (COSQC). (1984). *Iraqi Specification No. 45: Natural sources for gravel used in concrete and construction*. COSQC.

Central Organization for Standardization and Quality Control (COSQC). (2018). *Iraqi Specification No. 1703: Water used for concrete*. COSQC.

Fan, S., Zhang, Y., Ma, Y. X., & Tan, K. H. (2022). Strut-and-tie and finite element modelling of unsymmetrically-loaded deep beams. *Structures, 36*, 805–821.

Gao, Y. B., Chen, Z. L., Li, J. G., Hu, X. D., Shi, X. J., Sun, Z. M., ... & He, J. (2014). Genetic landscape of esophageal squamous cell carcinoma. *Nature Genetics, 46*(10), 1097–1102.

Jamali, D., & Neville, B. (2011). Convergence versus divergence of CSR in developing countries: An embedded multi-layered institutional lens. *Journal of Business Ethics, 102*, 599–621.

Karimizadeh, H., & Arabzadeh, A. (2021). A STM-based analytical model for predicting load capacity of deep RC beams with openings. *Structures, 34*, 1185–1200.

Mohammedali, T. K., Jalil, A. M., Abdul-Razzaq, K. S., & Mohammed, A. H. (2019). STM experimental verification for reinforced concrete continuous deep beams. *International Journal of Civil Engineering and Technology, 10*(2), 2227–2239.

Naaman, A., & Jeong, M. (1995). Structural ductility of concrete beams prestressed with FRP tendons. In *Non-Metallic (FRP) Reinforcement for Concrete Structures: Proceedings of the Second International RILEM Symposium (FRPRCS-2)* (Vol. 379). CRC Press.

Park, R. (1988). Ductility evaluation from laboratory and analytical testing. In *Proceedings of the 9th World Conference on Earthquake Engineering* (Vol. 8, pp. 605–616). Tokyo–Kyoto, Japan.

Shakir, Q. M., & Abd, B. B. (2020). Retrofitting of self-compacting RC half joints with internal deficiencies by CFRP fabrics. *Journal Teknologi (Sciences & Engineering), 82*(6), 49–62.

Shakir, Q. M., & Alghazali, A. F. (2024). Behavior of arched hybrid sustainable precast deep beams including green concrete. *Journal of Materials and Engineering Structures, 11*(1), 5–20.

Shakir, Q. M., & Hanoon, H. K. (2023). Behavior of high-performance reinforced arched-hybrid self-compacting concrete deep beams. *Journal of Engineering Science and Technology, 18*(1), 792–813.

Silveira, M. V., Bitencourt, L. A., & Das, S. (2022). A performance-based optimization framework applied to a classical STM-designed deep beam. *Structures, 41*, 488–500.

Yang, K. H., & Ashour, A. F. (2011). Aggregate interlock in lightweight concrete continuous deep beams. *Engineering Structures, 33*(1), 136–145.

Author(s) Information

Hussain K. Hashim
University of Misan
Amarah, Misan, Iraq
Contact e-mail: *enghs2301@uomisan.edu.iq*

Abdulkhaliq A. Jaafer
University of Misan
Amarah, Misan, Iraq

Hayder AL-Khazraji
University of Misan
Amarah, Misan, Iraq

To cite this article:

Hashim, H.K, Jaafer, A.A., & AL-Khazraji, H. (2025). Investigation of the efficacy of steel section reinforcement in hybrid deep beam applications. *The Eurasia Proceedings of Science, Technology, Engineering and Mathematics (EPSTEM), 37,* 150-162.